REKAYASA 23 (1) (2025): 41-56

REKAYASA

Jurnal Penerapan Teknologi dan Pembelajaran

http://journal.unnes.ac.id/journals/rekayasa

Performance Analysis of 18-Slot 12-Pole Ring-Type Orbital Electric Motor With Variations of Neodymium and Low-Carbon Steel Rotors Using Femm 4.2 Software

Widya Aryadi*[1], Michael Putra Julian Valentino[1], Esa Apriaskar[2]

[1]Department of Mechanical Engineering, Universitas Negeri Semarang, Semarang, Indonesia
[2]School of Electrical and Electronic Engineering, University of Sheffield, England

*Email: widyaaryadi@mail.unnes.ac.id

DOI: https://doi.org/10.15294/rekayasa.v23i1.38037

Abstract

This study aims to evaluate the performance of a ring-type orbital electric motor by examining the effects of variations in magnet position and configuration on flux linkage, force, and torque, and by comparing the results with those of a radial electric motor. The method employed is a 2D numerical simulation using FEMM 4.2 software. The design variations include the use of 0% (Pure) permanent magnets as well as magnets with lamination levels of 25%, 35%, and 50% for the orbital motor type. The simulation results indicate that the orbital motor with 0% (Pure) permanent magnets achieves the highest flux linkage of 3.13 Weber and the highest maximum torque of 336 Nm. For maximum force, the orbital motor with 25% laminated magnets shows the best result at 5207 N. Conversely, the radial motor with 0% (Pure) permanent magnets exhibits the lowest performance across all three parameters. Additionally, increasing the magnet lamination percentage does not always improve performance, as a decline is observed at 50% lamination. Overall, the orbital motor demonstrates superior performance compared to the radial motor.

Keywords: configuration, lamination, magnet position, performance, solidworks 2021

INTRODUCTION

Brushless Direct Current (BLDC) motor is one type of DC motor that uses permanent magnets as its main component. These advantages have made it a preferred option in numerous applications. These advantages include its simple structure, lightweight design, wide speed range, quiet operation, maintenance-free characteristics, accurate and precise control, and high dynamic response (Khan-Ngern et al., 2018; Utomo, 2020). Nevertheless, BLDC motors exhibit limitations in efficiency, particularly in producing low torque. This issue arises from the misalignment of the magnetic field direction between the stator and the rotor, caused by the stator windings not fully surrounding the rotor or vice versa (Kuczmann, 2024). Consequently, the magnetic field does not entirely occupy the toroidal core, leading to a decrease in motor

efficiency (Mostaman, 2023).

Previous studies on electric motor performance have been extensively conducted; however, several research gaps still remain. Jategaonkar et al. (2020) demonstrated that the selection of permanent magnet materials, particularly Neodymium Iron Boron (NdFeB), significantly affects motor efficiency, although their study did not analyze in depth the influence of magnet shape and geometry. Mudilulail & Kholistianingsih, (2024) evaluated the performance of a generator with a radial flux structure using finite element analysis, but the investigation was limited to output voltage and efficiency analysis without explicitly detailing force and torque characteristics. Meanwhile, Aslan et al. (2020) integrated electromagnetic and thermal modeling approaches in the design of an Interior Permanent Magnet (IPM) motor, yet the study did not address the effects of design parameter variations on the motor's dynamic performance.

Based on the issues outlined above, the researchers propose and develop an alternative electric motor design, namely an orbital ring-type electro motor with a low-carbon rotor (Wandika & Faridah, 2025). The use of rotor materials composed of alternating layers of low-carbon steel and aluminum, combined with a reduction in slots and neodymium usage, represents a new innovation in this study (Ahmed & Salleh, 2024). The purpose of reducing rotor material is to lower production costs without compromising motor performance, incorporating parameters such as the number of windings and current strength into the simulation—based on values from previous studies—to maintain consistency in comparison (Fischbacher et al., 2018; Zheng et al., 2022). It is expected that this design can generate ideal torque output and enable mass production. Although previous studies have analyzed this motor type, several shortcomings necessitate a re-evaluation (Hao et al., 2022; Islam et al., 2022).

In this research, the performance of the developed orbital ring-type electro motor is compared with that of a radial ring-type motor using FEMM 4.2 simulation, which employs the Finite Element Analysis (FEA) method to conduct testing without the need for physical prototypes. The initial design was created using SolidWorks 2021 and subsequently tested through 2D simulations in FEMM 4.2 to obtain motor performance data, including flux linkage, electromagnetic force, and generated torque (Sudirman, 2023).

This study aims to evaluate the performance of the developed orbital ring-type electro motor, compare it with the radial ring-type motor, and identify rotor and magnet configurations capable of producing optimal torque and electromagnetic force performance while maintaining efficiency and potential for mass production.

METHOD

This study employs a quantitative approach with an experimental simulation-based research design, in which data are collected in the form of numerical values and graphs, then processed logically to draw conclusions. The research focuses on the simulation of two ring-type electric motor models, an orbital electro motor and a radial electro motor, which were initially designed as 3D models using SolidWorks 2021 before being converted into 2D geometries through FEMM 4.2 for analysis purposes as shown in Figure 1. Parameters such as the number of windings, current, voltage, and input power were controlled throughout the simulation to produce outputs in the form of numerical data and performance graphs, including flux linkage, electromagnetic force, and torque (Cai

et al., 2021; Gmyrek, 2024). This virtual simulation method offers several advantages, including time and cost efficiency, testing flexibility, and minimal operational risk, while also enabling early-stage design verification and optimization to enhance product development effectiveness and reduce potential technical or financial errors.

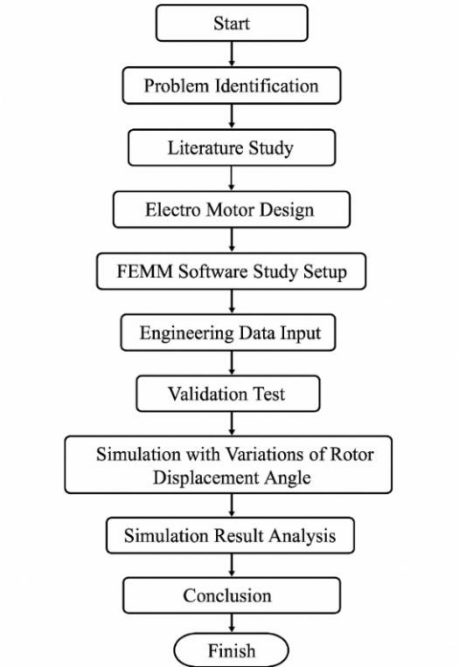

Figure 1. Research Flow Chart

Electro Motor Design

The 3D visual design of the orbital ring-type electro motor and the radial ring-type electro motor with a low-carbon steel rotor was developed using SolidWorks 2021 shown in Figure 2 (a) and (b). This design process includes a comprehensive visualization of each motor component, including the stator, rotor, and the ring configuration as well as the coil windings.

Rotor Deisgn Variations

The rotor design variations for orbital electric motor focus on configurations with Neodymium magnet lamination levels of 0%, 25%, 35%, and 50% shown in Figure 3 (a)-(d). Partial replacement of the magnets is carried out alternately using low-carbon steel and aluminum. The design was developed using SolidWorks 2021 to support the analysis of how magnet substitution affects motor performance through Finite Element Method (FEM)-based simulations (Ali et al., 2020). The following are the rotor designs corresponding to each Neodymium magnet lamination percentage.

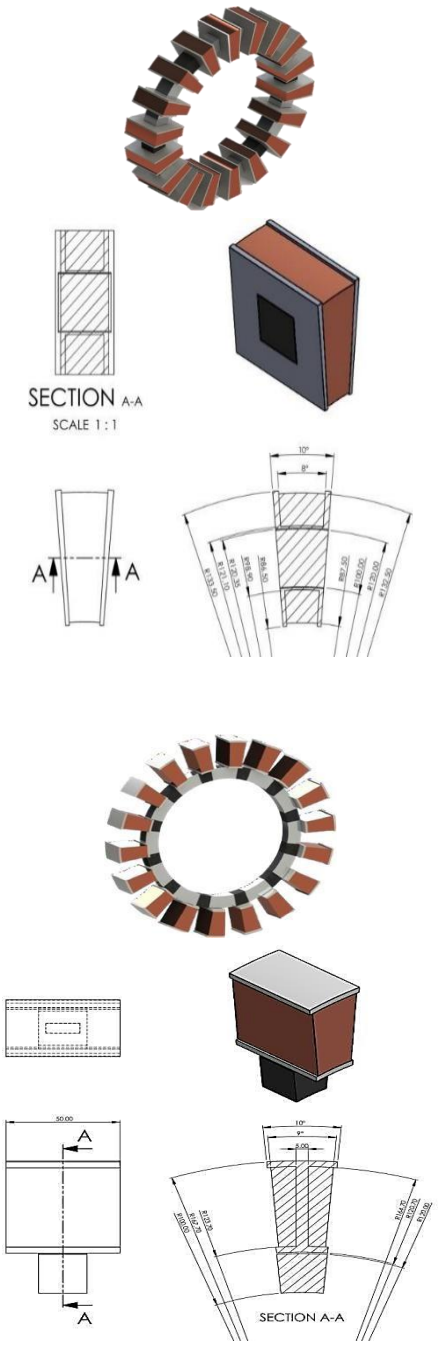

Figure 2. Design and Size with 18-slot, 12-pole of (a) Orbital Electric Motor (b) Radial Electric Motor

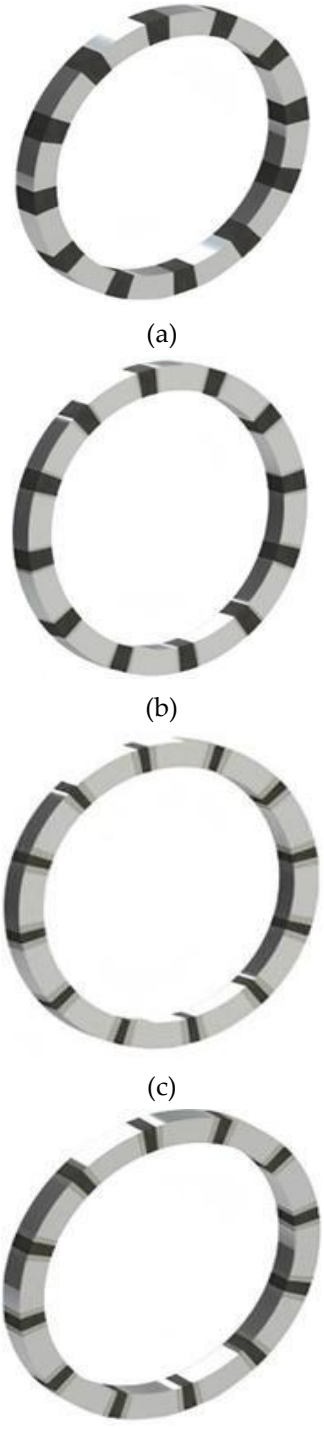

(a) (b) (c) (d)

Figure 3. Rotor Design of (a) 0% Lamination 0% Pure, (b) 25% Lamination, (c) 35% Lamination, (c) 50% Lamination.

Simulation Input Data

The input data used throughout the simulation include several key parameters such as the number of coil windings, battery current, supply voltage, and output power. These parameters are incorporated into the simulation input set and serve as the basis for generating numerical results, including torque, electromagnetic force, and flux linkage produced by the motor (Azahari et al., 2023; Gierczak et al., 2022). The table of input data used in the simulation is shown in Table 1.

Table 1. Simulation Input Data

Property	Value
Number of Slot	18
Number of Pole	12
Number of Windings	400
Current (Battery)	46,5 A
Voltage	72 V
Property	Value

Material Selection

The objective of material selection for this simulation is to represent the physical and mechanical properties of each material as realistically as possible under actual operating conditions. The materials were chosen carefully to ensure that the simulation results accurately reflect the motor's performance, particularly in terms of magnetic flux distribution, electromagnetic force, and the torque produced. The following materials were utilized and incorporated into the simulation process shown in Table 2.

.**Table 2.** Material Selection

Component	Material
Slot	ABS Plastic
Coil Winding	*Copper* 10 SWG
Rotor	*Low carbon steel* 1018, 1100 *aluminium alloy*, dan *Neodymium Sintered* NdeB

Finite-Element Method Simulation

The testing was carried out through simulation using Computer Aided Engineering (CAE) and the Finite Element Method (FEM).

This simulation-based approach offers several advantages, including the absence of physical maintenance costs, a broad range of testable parameters, improved computational accuracy, efficient execution time, and reduced risk of workplace accidents. In general, the finite element method applied in this simulation consists of three main stages: the pre-processing phase (model preparation and input data setup), the solution phase (numerical computation and processing), and the post-processing phase (result analysis and visualization). All of these stages were conducted systematically to ensure that the simulation outcomes can serve as valid references for evaluating the performance of the electric motor under investigation.

RESULT AND DISCUSSION

Design and Specification

The development of the electric motor design is based on the ring-type orbital electro motor, a newly proposed electric motor configuration. The radial motor design, on the other hand, is derived from an established conventional model. A previous study by Kwon et al., (2017) utilised a 2D model, as illustrated in the following Figure 4.

An evaluation of the previous design serves as an important consideration in determining the development steps undertaken in this study. This research analyzes and compares the performance of a ring-type orbital electro motor with that of a radial electro motor. The data obtained from simulation are used as the basis for comparison, particularly focusing on force, torque, and flux linkage parameters. The specifications of the design used in this study are presented in the following Table 3-5.

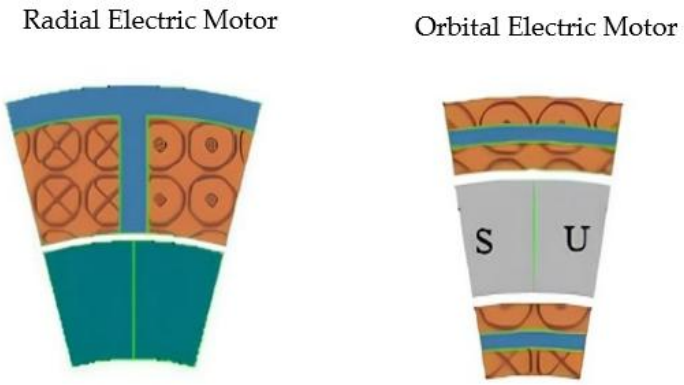

Figure 4. Radial Electric Motor and Orbital Electric Motor

Table 3. Specification of Electric Motor Size

Component	Size	
	Orbital (mm)	**Radial (mm)**
Outer armature diameter	267	334
Inner armature diameter	172	240
Armature width	30	30
Magnet thickness	20	20
Magnet width	20	20
Air gap	0,7	0,7

Table 4. Material Specification of Electric Motor

Component	Material
Magnet	*Neodymium Sintered* NdeB N35
Coil Winding	*Copper* 10 SWG
Armature/Housing	ABS Plastic

Table 5. Specification of Boundary Condition

Parameter	Value	Unit
Current	46,5	Ampere (A)
Voltage	72	Volt (V)
Number of Coil Winding	400	

Design Development

The design development was carried out on the ring-type orbital electro motor with reference to the design from previous studies. This development includes modifications to slot position, slot quantity, slot dimensions, and changes in rotor materials within the simulation process as shown in Figure 5. The main objective of this development is to obtain more accurate and optimized simulation results. In this study, the differences include adjustments to the rotor angle and the selection of rotor materials. These modifications aim to evaluate motor performance and determine the most efficient rotor configuration. To ensure data consistency, parameters such as the number of windings (400 turns) and the input current (46.5 A) were aligned with those used in earlier research (Ehya et al., 2021; Choudhary et al., 2019).

imulation Results

a. Linkage Flux

All motor configurations indicate that the maximum force is achieved when the rotor is positioned at an angle of –6° as shown in Figure 6 and Table 6. The orbital motor with 25% laminated permanent magnets delivers the highest performance, producing a maximum force of 5207 Newtons (N), surpassing all other configurations. Following this, the motor with 35% magnet lamination records a maximum force of 5073 N, while the orbital motor with 0% (Pure) permanent magnets generates 4971 N. Meanwhile, the orbital motor with 50% lamination shows a decrease in performance, with a maximum force of 4812 N. In contrast, the radial motor with 0% (Pure) permanent magnets exhibits the lowest performance, achieving a maximum force of only 3378 N.

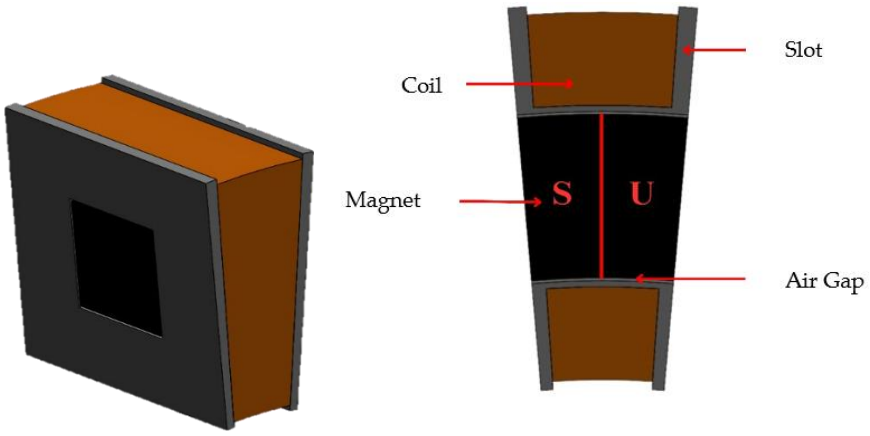

(a) (b)

Figure 5. Design Development Orbital Electric Motor of Ring Type (a) 3D, (b) 2D

The graph shows that all five curves exhibit a sinusoidal pattern, indicating that the generated force experiences periodic fluctuations as the rotor displacement angle changes. The curve of the orbital motor with 0% (Pure) neodymium magnets (blue line) demonstrates the most stable variation compared to the other motor types. These findings suggest that applying a certain level of magnet lamination in orbital motors can significantly enhance force performance, particularly at a rotor angle of −6°. However, increasing the lamination percentage to 50% does not necessarily correspond to higher output force and instead tends to reduce the maximum force. This indicates that the optimization of lamination levels must be carefully considered to achieve efficient motor performance for a given configuration (Albazzan et al., 2019). Magnetic Flux Line Orientation at A Rotor Shift Variation of −6º shown in Figure 7.

Table 6. Force Performance Results

Variation of Degree (º)	Force (N)				
	Orbital 0%	Orbital 25%	Orbital 35%	Orbital 50%	Radial 0%
-10	3735	3394	3206	2911	2736
-9	4248	3988	3795	3481	2861
-8	4688	4588	4401	4080	3047
-7	4944	5022	4856	4558	3250
-6	**4971**	**5207**	**5073**	**4812**	**3378**
-5	4757	5122	5015	4796	3234
-4	4294	4763	4676	4484	2577
-3	3568	4106	4039	3862	1795
-2	2586	3108	3062	2910	962
-1	1355	1711	1681	1561	408
0	1,7	1,07	1,9	6,5	16
1	1319	1526	1433	1128	666
2	2507	2758	2609	2134	1304
3	3466	3673	3458	2861	1988
4	4165	4279	3993	3274	2598
5	4626	4593	4216	3372	2785
6	4825	4624	4149	3139	2547
7	4811	4363	3773	2658	2171
8	4569	3810	3191	2185	1744
9	4147	3178	2643	1814	1311
10	3647	2650	2215	1544	1069

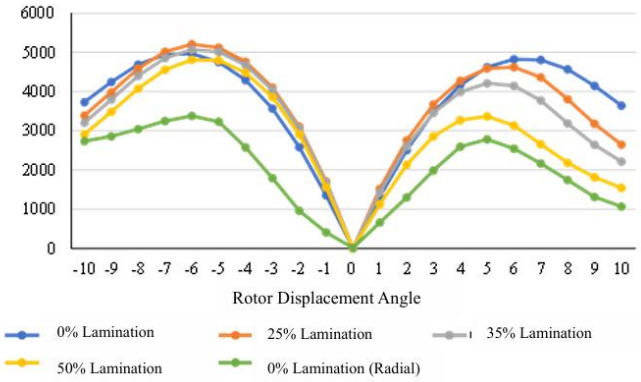

Figure 6. Graph of Force Output

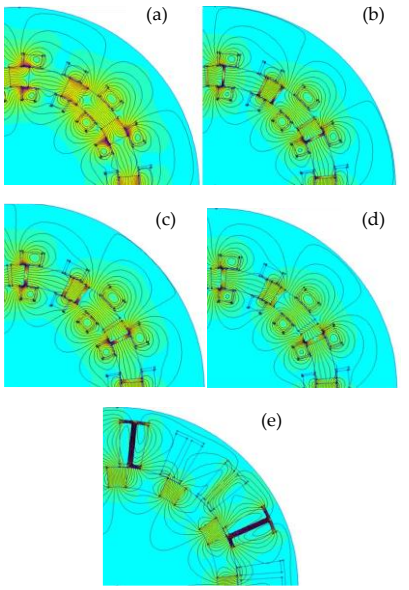

Figure 7. Magnetic Flux Line Orientation at A Rotor Shift Variation of −6º. (a) Orbital Magnet with 0% Lamination, (b) Orbital with 25% Lamination, (c) Orbital with 35% Lamination, (d) Orbital with 50% Lamination, (e) Radial Magnet with 0% Lamination.

b. Torque

The torque simulation results for the orbital electro ring-type motor are presented based on five test configurations: an orbital motor with 0% (Pure) neodymium magnets, orbital motors with 25%, 35%, and 50% laminated neodymium magnets, and a radial motor with 0% (Pure) neodymium magnets. All simulation data were compiled into numerical tables to describe the torque performance of each motor variation, and subsequently visualized in the form of line graphs to facilitate interpretation of torque changes resulting from variations in rotor displacement angle as shown in Table 7. Through this graphical visualization, the patterns and trends of torque variation for each motor configuration can be identified more clearly, allowing researchers to draw conclusions regarding the influence of rotor displacement angle on motor performance.

The simulations were conducted in two stages—single-phase (1-phase) and three-phase (3-phase) current testing—in order to compare performance differences and to ensure the accuracy of the simulation results in accordance with established methodological principles.

All motor configurations exhibit sinusoidal torque curves consistent with electromagnetic operating principles, where the torque value increases as the rotor position shifts and subsequently decreases when the rotor magnet approaches the current-carrying stator slots as shown in Figure 8. The orbital motor with 25% laminated magnets produces the highest maximum torque, reaching 202 Nm at a rotor position of 6°, followed by the orbital motor with 0% (Pure) permanent magnets, which achieves a peak torque of 200 Nm at 7°. Meanwhile, the configurations with 35% and 50% lamination generate maximum torques of 196 Nm and 186 Nm, respectively, both occurring at a rotor angle of 6°. The radial motor with 0% (Pure) permanent magnets shows the lowest performance, producing a maximum torque of 110 Nm at the same angular position.

Table 7. Torque Performance Results with Current Applied to 1-Phase

Variation of Degree (º)	Torque (Nm)				
	Orbital 0%	Orbital 25%	Orbital 0%	Orbital 50%	Orbital 0%
-9	178	-9	178	-9	178
-8	190	-8	190	-8	190
-7	196	-7	196	-7	196
-6	193	-6	193	-6	193
-5	182	-5	182	-5	182
-4	163	-4	163	-4	163
-3	134	-3	134	-3	134
-2	96	-2	96	-2	96
-1	50	-1	50	-1	50
0	0.1	0	0.1	0	0.1
1	52	1	52	1	52
2	100	2	100	2	100
3	138	3	138	3	138
4	168	4	168	4	168
5	187	5	187	5	187
6	198	6	198	6	198
7	**200**	7	**200**	7	**200**
8	194	8	194	8	194
9	182	9	182	9	182

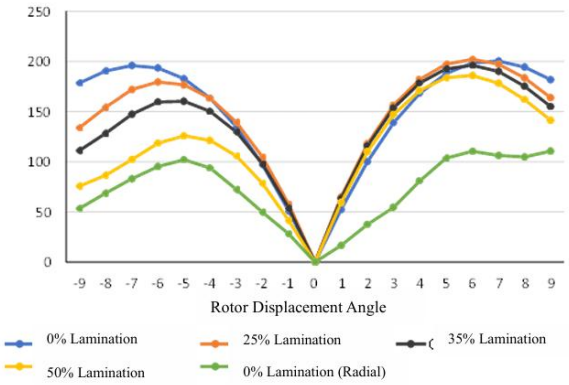

Figure 8. Torque Output Graph with Current Applied to 1-Phase

The orbital motor with a 0% 0% (Pure) permanent-magnet rotor demonstrates the highest maximum torque, reaching 336 Nm at a rotor position of 8°, followed by the 25% laminated configuration at 296 Nm, the 35% laminated configuration at 277 Nm, and the 50% laminated configuration at 247 Nm at 6° as shown in Table 8. Meanwhile, the radial motor with 0% (0% (Pure)) permanent magnets records the lowest maximum torque, producing only 156 Nm at 6°. The orbital motor with 0% (0% (Pure)) magnets not only achieves the highest peak torque but also exhibits more stable torque fluctuations across rotor angle variations, indicating a more consistent electromagnetic response to positional changes as shown in Figure 9. This stability is closely linked to the tangential force acting perpendicular to the rotation axis, which directly contributes to torque generation, with the 8° position representing the optimal condition where magnetic field interaction and current flow achieve maximum rotational efficiency (Bazzo et al., 2021; Chen et al., 2025). Magnetic flux line orientation for different rotor-shift variations shown in Figure 10.

Table 8. Torque Performance Results With 3-Phase Current

Variation of Degree (º)	Torque (Nm)				
	Orbital 0%	Orbital 25%	Orbital 0%	Orbital 50%	Orbital 0%
-20	331	-20	331	-20	331
-19	332	-19	332	-19	332
-18	334	-18	334	-18	334
-17	332	-17	332	-17	332
-16	325	-16	325	-16	325
-15	317	-15	317	-15	317
-14	329	-14	329	-14	329
-13	335	-13	335	-13	335
-12	336	-12	336	-12	336
-11	333	-11	333	-11	333
-10	331	-10	331	-10	331
-9	332	-9	332	-9	332
-8	334	-8	334	-8	334
-7	332	-7	332	-7	332
-6	325	-6	325	-6	325
-5	317	-5	317	-5	317
-4	329	-4	329	-4	329
-3	335.	-3	335.	-3	335.
-2	336	-2	336	-2	336
-1	333	-1	333	-1	333
0	331	0	331	0	331
1	332	1	332	1	332
2	334	2	334	2	334
3	332	3	332	3	332
4	325	4	325	4	325
5	317	5	317	5	317
6	329	6	329	6	329
7	335	7	335	7	335
8	**336**	8	**336**	8	**336**
9	333	9	333	9	333
10	331	10	331	10	331
11	332	11	332	11	332
12	334	12	334	12	334
13	332	13	332	13	332
14	325	14	325	14	325
15	317	15	317	15	317
16	329	16	329	16	329
17	335	17	335	17	335
18	336	18	336	18	336
19	333	19	333	19	333
20	331	20	331	20	331

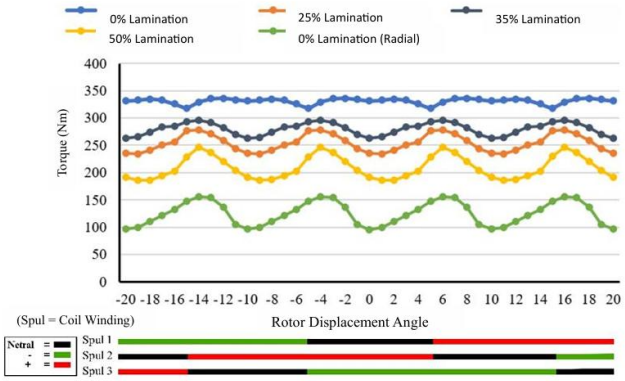

Figure 9. Torque Output Graph with 3-Phase Current

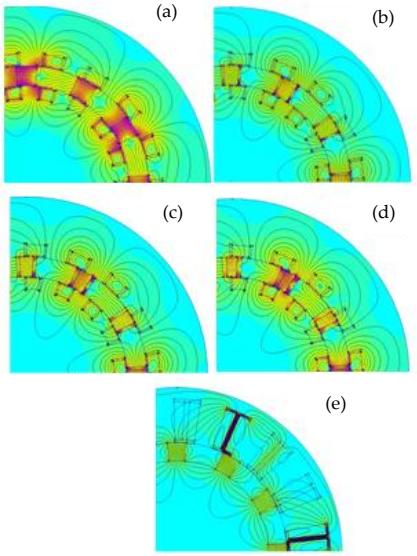

Figure 10. Magnetic Flux Line Orientation For Different Rotor-Shift Variations: (a) 0% (0% (Pure)) orbital magnet at 8°, (b) orbital lamination 25% at 6°, (c) orbital lamination 35% at 6°, (d) orbital lamination 50% at 6°, and (e) 0% (0% (Pure)) radial magnet at 6°.

Discussion

Based on the FEMM 4.2 simulation results, the orbital motor with 0% (0% (Pure)) magnets produced the highest flux linkage among all design variations. The performance ranking places the 0% (0% (Pure))-magnet orbital configuration first, followed by the 25% laminated and 35% laminated designs. Notably, the radial motor with 0% (0% (Pure)) magnets ranked fourth yet still outperformed the orbital motor with 50% lamination. These findings indicate that the use of 0% (0% (Pure)) magnets—particularly in the orbital design—significantly increases the magnetic flux density passing through the coil windings (Potgieter et al., 2016). This aligns with the fundamental principle of flux linkage: the greater the magnetic flux captured by the coil, the more electromagnetic energy can be converted into mechanical output as shown in Figure 11.

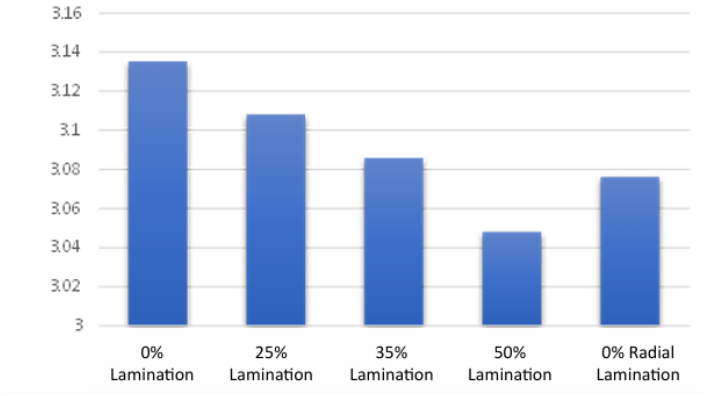

Figure 11. Maximum Flux-Linkage Performance Graph

Simulation results show that the orbital motor with 25% laminated magnets produces the highest maximum force among all configurations, followed by the 35% laminated version and the 0% (Pure)-magnet design. This indicates that an optimal level of lamination can enhance the motor's thrust effectiveness (Hammoodi et al., 2020). The trend aligns with the electromagnetic force equation, where force is proportional to the magnetic flux density (B) acting on the conductor windings. The 25% and 35% laminated configurations appear to provide a balanced concentration and stability of the magnetic flux delivered to the rotor. In contrast, the radial motor with 0% (Pure) magnets yields the lowest force output, suggesting that the radial design is less effective in optimizing magnetic-field distribution for achieving maximum force as shown in Figure 12.

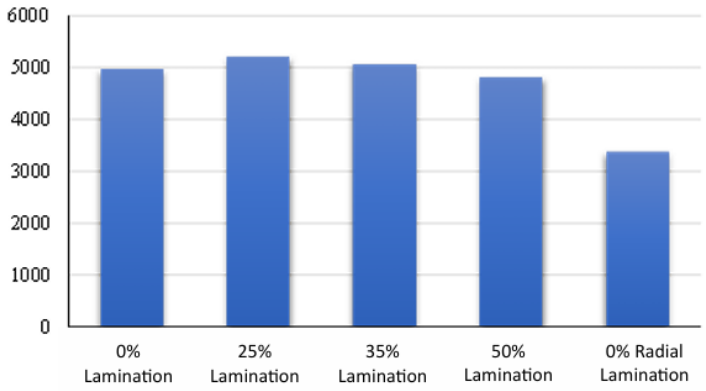

Figure 12. Maximum Force Performance Graph

The torque simulation results show that the orbital motor with 0% (Pure) magnets achieves the highest maximum torque, followed sequentially by the 25%, 35%, and 50% laminated-magnet orbital motors, with the radial motor using 0% (Pure) magnets ranking last. This indicates that the 0% (Pure)-magnet orbital design enables a stronger and more concentrated magnetic interaction along the rotational axis (Grytsiuk et al., 2020; Khomskii & Streltsov, 2020). In the context of tangential force generation, rotor geometry, magnet placement, and flux concentration play a critical role in determining torque output (Humphries et al., 2017; Amin & Stiles, 2016). The rotor in the 0% (Pure)-magnet orbital motor is designed to interact with the electromagnetic field for a longer duration and over a wider effective area, resulting in greater

and more stable torque production as shown in Figure 13.

Compared with the previous study by Fachrezi (2024), which employed an orbital electro motor with a 21-slot and 21-magnet rotor configuration, the motor developed in this work exhibits slightly lower performance in terms of flux linkage and torque but shows a substantial improvement in generated force. As summarized in Table 9, the peak force in Fachrezi's study reached 3726 N, whereas the highest force obtained in this study was 5207 N for the orbital motor using 25% laminated neodymium magnets. In terms of flux linkage, the previous research reported 8.75 Wb, while the highest value in this study was 3.13 Wb for the 0% (Pure) permanent-magnet configuration. For torque, the earlier work achieved 469.84 Nm, whereas this study recorded a maximum of 336 Nm. Overall, among the five rotor material variations evaluated, the 0% (Pure) permanent-magnet orbital motor demonstrates the most optimal efficiency.

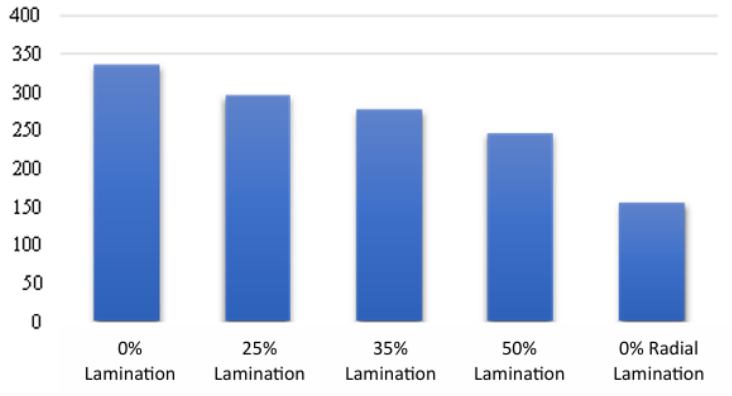

Figure 13. Maximum Torque Performance Graph

Table 9. Simulation Results of The Orbital Electric Motor with 21 Slots and 21 Poles

Variasi of Degree	Linkage Flux (Wb)	Force (N)	Torque (Nm)
-10	7,08	1404	148,40
-9	7.01	848	43,40
-8	7.01	899	57,97
-7	7,10	1506	164,11
-6	7,27	2325	279,85
-5	7,51	3138	389,93
-4	7,82	3674	461,46
-3	8,16	3726	469,84
-2	8,46	3166	395,28
-1	8,67	1983	232,30
0	**8,75**	864	0,13
1	8,67	1983	232,30
2	8,46	3166	395,28
3	8,16	**3726**	**469,84**
4	7,82	3674	461,46
5	7,51	3138	389,93
6	7,27	2325	279,85
7	7,10	1506	164,11
8	7.01	899	57,97
9	7.01	848	43,40
10	7,08	1404	148,40

CONCLUSION

Based on the results and analysis obtained, it can be concluded that the objectives of this study have been successfully achieved. The findings show that the orbital motor exhibits superior performance compared to the radial motor across flux linkage, electromagnetic force, and torque characteristics. The highest flux linkage of the orbital motor is achieved using a 0% (Pure) magnet configuration, reaching 3.13 Wb, which is higher than the radial motor's 3.08 Wb. The use of laminations progressively decreases the flux linkage, with values of 3.11 Wb (25% lamination), 3.08 Wb (35% lamination), and 3.05 Wb (50% lamination). Overall, the 0% (Pure)-magnet orbital motor demonstrates a 1.62% higher flux linkage than the radial motor, indicating a modest yet meaningful improvement in magnetic flux density. In terms of electromagnetic force, the orbital motor consistently outperforms the radial motor, achieving a maximum force of 5207 N at 25% lamination, which surpasses the radial motor's maximum force of 3378 N under the 0% (Pure) magnet configuration. The 0% (Pure)-magnet orbital motor produces 47.15% higher force compared to the radial motor, reflecting a significant advantage in electromagnetic efficiency. Furthermore, the orbital motor demonstrates a substantial improvement in torque, reaching a maximum of 336 Nm in the 0% (Pure) magnet configuration, in contrast to the radial motor's 156 Nm. Even with increasing lamination levels (25%, 35%, and 50%), the orbital motor maintains higher torque values of 296 Nm, 277 Nm, and 247 Nm, respectively. Overall, the 0% (Pure)-magnet orbital motor delivers 115.4% greater torque than the radial motor, indicating a markedly superior rotational performance.

REFERENCES

Ahmed, W. H., & Salleh, M. S. (2024). A review on tool pin geometry of friction stir welding. *Al-Khwarizmi Engineering Journal*, *20*(2), 39-55.

Albazzan, M. A., Harik, R., Tatting, B. F., & Gürdal, Z. (2019). Efficient design optimization of nonconventional laminated composites using lamination parameters: A state of the art. *Composite Structures*, *209*, 362-374.

Ali, S. M., Ali, Z. J., & Abd, M. M. (2020). Design and modeling of a soft artificial heart by using the SolidWorks and Ansys. In *IOP Conference Series: Materials Science and Engineering*, *671*(1), 012062.

Amin, V. P., & Stiles, M. D. (2016). Spin transport at interfaces with spin-orbit coupling: Formalism. *Physical Review B*, *94*(10), 104419.

Aslan, M., Özpolat, A. B., İşçi, C., Eroğlu, F., & Vural, A. M. (2020). Design and modelling of internal permanent magnet motor. *The International Journal of Energy and Engineering Sciences*, *5*(2), 80-104.

Azahari, F. T., Atel, M. N. A., Samsuri, S. S., & Aziz, A. A. (2023). The Conceptual Design of An Electro-Magnetic Power Generator. *Semesta Teknika*, *26*(2), 231-239.

Bazzo, T. D. P. M., Moura, V. D. O., & Carlson, R. (2021). A step-by-step procedure to perform preliminary designs of salient-pole synchronous generators. *Energies*, *14*(16), 4989.

Cai, W., Wu, X., Zhou, M., Liang, Y., & Wang, Y. (2021). Review and development of electric motor systems and electric powertrains for new energy vehicles. *Automotive Innovation*, *4*(1), 3-22.

Chen, K., Ma, S., Li, C., Wu, Y., & Ma, J. (2025). Optimization and Design of Built-In U-Shaped Permanent Magnet and Salient-

Pole Electromagnetic Hybrid Excitation Generator for Vehicles. *Symmetry*, *17*(6), 897.

Choudhary, A., Goyal, D., Shimi, S. L., & Akula, A. (2019). Condition Monitoring and Fault Diagnosis of Induction Motors: A Review: A. Choudhary et al. *Archives of Computational Methods in Engineering*, *26*(4), 1221-1238.

Ehya, H., Skreien, T. N., & Nysveen, A. (2021). Intelligent data-driven diagnosis of incipient interturn short circuit fault in field winding of salient pole synchronous generators. *Transactions on Industrial Informatics*, *18*(5), 3286-3294.

Fischbacher, J., Kovacs, A., Gusenbauer, M., Oezelt, H., Exl, L., Bance, S., & Schrefl, T. (2018). Micromagnetics of rare-earth efficient permanent magnets. *Journal of Physics D: Applied Physics*, *51*(19), 193002.

Gierczak, M., Markowski, P. M., & Dziedzic, A. (2022). The modeling of magnetic fields in electromagnetic microgenerators using the finite element method. *Energies*, *15*(3), 1014.

Gmyrek, Z. (2024). Optimal Electric Motor Designs of Light Electric Vehicles: A Review. *Energies*, *17*(14), 3462.

Grytsiuk, S., Hanke, J. P., Hoffmann, M., Bouaziz, J., Gomonay, O., Bihlmayer, G., ... & Blügel, S. (2020). Topological–chiral magnetic interactions driven by emergent orbital magnetism. *Nature communications*, *11*(1), 511.

Hammoodi, S. J., Flayyih, K. S., & Hamad, A. R. (2020). Design and implementation speed control system of DC motor based on PID control and matlab simulink. *International Journal of Power Electronics and Drive Systems*, *11*(1), 127-134.

Hao, Z., Ma, Y., Wang, P., Luo, G., & Chen, Y. (2022). A review of axial-flux permanent-magnet motors: topological structures, design, optimization and control techniques. *Machines*, *10*(12), 1178.

Humphries, A. M., Wang, T., Edwards, E. R., Allen, S. R., Shaw, J. M., Nembach, H. T., ... & Fan, X. (2017). Observation of spin-orbit effects with spin rotation symmetry. *Nature communications*, *8*(1), 911.

Islam, Z., Khan, F., Ullah, B., Milyani, A. H., & Ahmed Azhari, A. (2022). Design and analysis of three phase axial flux permanent magnet machine with different PM shapes for electric vehicles. *Energies*, *15*(20), 7533.

Jategaonkar, A., Ramesh, P., Kochgabay, P., & Lenin, N. C. (2020). Electromagnetic and thermal analysis of permanent magnet BLDC wiper motor. *Advances in Electrical Control and Signal Systems: Select Proceedings of AECSS 2019*, 405-414.

Khan-Ngern, W., Keyoonwong, W., Chatsiriwech, N., Sangnopparat, P., Mattayaboon, P., & Worawalai, P. (2018). High performance BLDC motor control for electric vehicle. *International Conference on Engineering, Applied Sciences, and Technology (ICEAST)*, 1-4.

Khomskii, D. I., & Streltsov, S. V. (2020). Orbital effects in solids: Basics, recent progress, and opportunities. *Chemical Reviews*, *121*(5), 2992-3030.

Kuczmann, M. (2024). Review of DC motor modeling and linear control: Theory with laboratory tests. *Electronics*, *13*(11), 2225.

Kwon, S. C., Jo, M. S., & Oh, H. U. (2017). Experimental Validation of Fly-Wheel Passive Launch and On-Orbit Vibration Isolation System by Using a Superelastic SMA Mesh Washer Isolator. *International Journal of Aerospace Engineering*, *2017*(1), 5496053.

Mostaman, A. (2023). Design Optimization and Analysis of Radial Flux Permanent Magnet Generator Using Local

Optimization Method. *El-Cezeri*, *11*(1), 58-64.

Mudilulail, S. A., & Kholistianingsih, K. (2024). Effect of Rotor Teeth Width Variations on Back EMF Constant of a 12-Slot 8-Pole Permanent Magnet Synchronous Generator: A Finite Element Analysis. *Applied Engineering, Innovation, and Technology*, *1*(1), 23-30.

Potgieter, J. H., Marquez-Fernandez, F. J., Fraser, A. G., & McCulloch, M. D. (2016). Effects observed in the characterization of soft magnetic composite for high frequency, high flux density applications. *Transactions on Industrial Electronics*, *64*(3), 2486-2493.

Sudirman, Z. (2023). Implementation of Solidworks Software Usage through Training to Enhance Vocational Students' Competence. *Butta Toa: Jurnal Pengabdian Kepada Masyarakat*, *1*(01), 41-47.

Wandika, M., & Faridah, L. (2025). Analysis of load on permanent magnet synchronous generator (pmsg) 12s8p with speed variation. *Jurnal Informatika dan Teknik Elektro Terapan*, *13*(1), 721-731.

Zheng, B., Fan, J., Chen, B., Qin, X., Wang, J., Wang, F., ... & Liu, X. (2022). Rare-earth doping in nanostructured inorganic materials. *Chemical Reviews*, *122*(6), 5519-5603.